*Molecular Vision* 2022; 28:378-393 <http://www.molvis.org/molvis/v28/378>
Received 4 October 2021 | Accepted 14 October 2022 | Published 16 October 2022



# Sulforaphane recovers cone function in an Nrf2-dependent manner in middle-aged mice undergoing RPE oxidative stress

**Xiaoping Qi,[1] Dorothy A. Walton,[2] Kendra S. Plafker,[2] Michael E. Boulton,[1] Scott M. Plafker[2]**

*[1]Department of Ophthalmology and Visual Sciences, University of Alabama at Birmingham (UAB), Birmingham, AL; [2]Aging and Metabolism Research Program, Oklahoma Medical Research Foundation, Oklahoma City, OK*

**Purpose:** Sulforaphane (SFN) is an isothiocyanate derived from cruciferous vegetables that has therapeutic efficacy in numerous animal models of human disease, including mouse models of retinal degeneration. However, despite dozens of clinical trials, the compound remains to be tested as a clinical treatment for ocular disease. Numerous cellular activities of SFN have been identified, including the activation of Nrf2, a transcription factor that induces a battery of target gene products to neutralize oxidative and xenobiotic stresses. As Nrf2 expression and function reportedly decrease with aging, we tested whether the loss of the transcription factor limits the therapeutic efficacy of SFN against retinal degeneration.
**Methods:** Six- to 8-month-old wild-type and Nrf2 knockout mice were treated with SFN beginning 1 month after ribozyme-mediated knockdown of superoxide dismutase 2 (SOD2) mRNA in the RPE. The impacts of MnSOD (the protein product of SOD2) knockdown and the efficacy of SFN were evaluated using a combination of electroretinography (ERG), spectral domain optical coherence tomography (SD-OCT), and postmortem histology.
**Results:** SFN restored the ERG photopic b-wave suppressed by MnSOD loss in wild-type mice, but not in the Nrf2 knockout mice. In contrast, ERG scotopic a- and b-wave loss was not restored for either genotype. SFN significantly improved retinal thickness in the Nrf2 knockout mice with MnSOD knockdown, but this was not observed in the wild-type mice. In both genotypes, SFN treatment reduced morphological markers of RPE atrophy and degeneration, although these improvements did not correlate proportionally with functional recovery.
**Conclusions:** These findings highlight the capacity of SFN to preserve cone function, as well as the potential challenges of using the compound as a standalone treatment for age-related retinal degeneration under conditions associated with reduced Nrf2 function.

1-isothiocyanato-(4R)-(methylsulfinyl) butane (SFN) is a phytochemical present in cruciferous vegetables, including broccoli, radishes, cabbage, and Brussels sprouts, with the highest concentrations found in broccoli sprouts [1]. This isothiocyanate is produced by plants in response to predation via the vesicular release of the hydrolytic enzyme myrosinase, which enters damaged cells and converts the precursor compound glucoraphanin into glucose and SFN [2]. This predation response is also elicited by chewing or heating these vegetables. The relatively high bioavailability of SFN is further promoted via myrosinase produced by microbiota resident in the human intestine [3].

Since the discovery of SFN in 1992 [4], the phytochemical has shown therapeutic efficacy in rodent models of human diseases ranging from arthritis and cancer to chronic obstructive pulmonary disease and autism (reviewed in [5,6]). These promising findings spurred dozens of clinical trials evaluating the compound, but to date, SFN has not received approval from the U.S. Food and Drug Administration (FDA). Confounding factors that may be limiting the clinical applications of SFN include dosing amounts and frequency, as well as formulations [6]. Compounding these challenges is the growing list of cellular proteins and pathways targeted by SFN. These include HDAC inhibition [7-12], induction of mitochondrial fusion [13], inhibition of Phase I metabolic enzymes [14], and induction of apoptosis [15-17]).

SFN has been extensively studied in the context of activating Nrf2, a master anti-stress transcription factor that regulates the expression of Phase II detoxification genes, antioxidant genes, and genes encoding enzymes of anabolic and bioenergetic pathways [18]. SFN stabilizes Nrf2 by thionoacylating multiple cysteines within KEAP1 [19-23], the substrate adaptor of a multisubunit E3 ligase that marks Nrf2 for proteasomal degradation [19,21,24]. SFN modification of KEAP1 liberates the KEAP1-Nrf2 complex from the E3 ligase, thus preventing Nrf2 from being marked for degradation with polyubiquitin chains. The stabilized transcription factor enters the nucleus and induces target gene expression. The protein products of Nrf2 target genes cooperatively maintain and restore redox and proteome homeostasis, making Nrf2 activation by SFN an attractive therapeutic option for diseases linked to unchecked oxidative stress, including those

Correspondence to: Scott M. Plafker, Aging and Metabolism Research Program, Oklahoma Medical Research Foundation, 825 NE 13th St, OKC, OK 73104; email: plafkers@omrf.org

impacting the retina (e.g., dry age-related macular degeneration [dAMD]) [25].

Preserving RPE cell function and integrity during aging is a long-standing treatment goal, as atrophy of this cell layer precipitates or accompanies photoreceptor loss during AMD development [26]. Whether SFN has clinical utility for AMD remains to be established in part because Nrf2 expression and Nrf2-mediated transcription can be compromised with aging. Dysmorphic macular RPE in postmortem AMD eyes have reduced expression of Nrf2 and Nrf2 target gene products [27,28], and the RPE cells of aged mice have impaired Nrf2 signaling [29]. Furthermore, cigarette smoking is the leading environmental risk factor for AMD and impairs Nrf2 signaling in an age-dependent manner [30].

In the present study, we directly tested whether Nrf2 is required for the therapeutic efficacy of SFN in a mouse model of retinal degeneration induced by RPE mitochondrial oxidative stress. This model uses a ribozyme to knockdown manganese superoxide dismutase (MnSOD) expression in the RPE of C57BL/6 mice, inducing pathologies consistent with those observed in AMD despite the lack of a macula in mice [31-33]. MnSOD localizes within mitochondria and dismutates superoxide produced by the electron transport chain into hydrogen peroxide ($H_2O_2$) and oxygen. The $H_2O_2$ is subsequently converted into oxygen and water. Suppressing MnSOD expression in the RPE layer leads to oxidative stress that alters RPE and choroidal morphology, increases autofluorescent bis-retinoids in extracellular deposits, and causes disorganization and loss of the RPE and underlying photoreceptors. These deficits reduce vision and ERG amplitudes [31-34]. Complementary work in which the SOD2 locus was genetically ablated from the RPE of either C57BL/6 or BALB/c mice using Cre-lox manipulation revealed a time-dependent progression of changes initiated by RPE oxidative stress. Subsequent pathological features observed included increased lipofuscin-associated autofluorescence, scotopic and photopic ERG deficits, reduced outer nuclear layer (ONL) thickness, increased RPE cell area in the central retina, disorganized mitochondrial cristae, decreased mitochondrial DNA content within the RPE, and compensatory upregulation of glycolytic enzymes, indicative of RPE cells switching from respiration to glycolysis [34,35]. Transition of the RPE to glycolysis deprives photoreceptors of sufficient glucose and underscores the metabolic interdependence and cooperation between the two cell types [36-40]. Similarly, SOD2 gene ablation from muscle decreases oxidative phosphorylation and upregulates the expression of several glycolytic enzymes [41].

In the present study, we used the SOD2 ribozyme knockdown approach in RPE cells to evaluate the efficacy of interventional SFN administration in mitigating disease pathologies in wild-type and Nrf2 knockout (KO) mice. Global Nrf2 KO mice have been valuable for elucidating the contributions of oxidative stress to the pathophysiology of a range of cancers as well as liver, lung, and kidney diseases (e.g., [42-45]). In the context of the RPE and neuroretina, Nrf2 knockout mice model aspects of wet and dry AMD in an age-dependent manner, with phenotypes manifesting primarily after 1 year of age [46]. To amplify these AMD-like phenotypes, investigators have coupled aged global Nrf2 knockout mice (i.e., 12–18 months old) with dietary manipulations (e.g., high-fat or high-glycemic diets) [47,48] or with co-knockout of peroxisome proliferator-activated receptor gamma coactivator-1α (PGC-1α) [49]. In the work reported here, Nrf2 KO mice were fed standard chow, and the studies were completed before mice reached 1 year of age to limit ocular deficiencies caused by absence of the transcription factor.

We report that administering SFN three times weekly to RPE-MnSOD knockdown mice beginning 1 month after SOD2 mRNA-targeting ribozyme injections restored cone function and improved morphological markers of RPE atrophy and degeneration. Notably, this efficacy was dependent on Nrf2 expression. These findings highlight the therapeutic utility of SFN to counter retinal degeneration, as well as potential limitations of the compound in scenarios of compromised Nrf2 expression and function.

## METHODS

*Materials:* Paraformaldehyde was obtained from Sigma-Aldrich Co. (St. Louis, MO). Antigen retrieval solution, Rodent Decloaker, 10X was purchased from Biocare Medical (Concord, CA). Rabbit anti-IBa1 was obtained from Wako Chemicals USA, Inc. (Richmond, VA; Catalog# 019–19741). Rat anti-F4/80 was purchased from ThermoFisher Scientific (Rockford, IL; Catalog# 14–4801–82), and the Alexa Fluor 594- and 488-tagged secondary antibody (goat anti-rabbit, Catalog # A35560; and goat anti-rat, Catalog # SA5–10018) were from Invitrogen (Carlsbad, CA). All sections were mounted with Vectashield medium from Vector Laboratories (Burlingame, CA). R- sulforaphane (SFN, Product ID S8048; Catalog# 142,825-10–3) was purchased from LKT Laboratories, Inc. (St. Paul, MN).

*Mice and injections of AAV1 knock down SOD2 and SFN:* All mouse experiments were performed in accordance with the guidelines of the Association for Research in Vision and Ophthalmology Statement for the Use of Animals in

Ophthalmic and Visual Research. Experimental procedures were approved by the University of Alabama Institutional Animal Care and Use Committee (IACUC# 21,271, Birmingham, AL). Wild-type C57BL/6J mice and Nrf2 KO mice (global KO) were obtained from Jackson (JAX) Laboratories (Bar Harbor, ME; strains #000664 and #017009, respectively). The Nrf2 KO mice were backcrossed into the C57BL/6J background and simultaneously screened for loss of retinal degeneration 8 (*rd8*). Ablation of the Nrf2 gene was confirmed with PCR (95˚C for 3 min,

95 ˚C for 15 s, 60 ˚C for 15 s, 72 ˚C for 45 s, 72 ˚C for 3 min 4 ˚C hold) using JAX-designed primers (common forward primer sequence: 5′-GCC TGA GAG CTG TAG GCC C-3′; wild-type reverse primer sequence: 5′-GGA ATG GAA AAT AGC TCC TGC C-3′; mutant reverse primer sequence: 5′-GAC AGT ATC GGC CTC AGG AA-3′. Mice were 6–8 months of age at the beginning of the study and 10–12 months old by the end of the study. The right eyes (OD) of the mice were injected subretinally with 0.5 µl of 2.5 × $10^{12}$ particles/ml of recombinant AAV1 constructs based on the pTR-UF2 vector expressing *SOD2*-specific hammerhead ribozyme, Rz432, driven by the RPE-specific VMD2 promoter (*AAV1-Rz-SOD2*), to drive ribozyme gene expression in the RPE layer as previously described [31]. The contralateral control eye (OS) was untreated. The total number of animals was 42, and they were separated into groups for untreated controls, untreated + sulforaphane (SFN), SOD2 KD, and SOD2 KD+ SFN. Each treatment group contained five to six mice. The mice were administered vehicle (PBS; Phosphate-Buffered Saline, pH7.4, 1X contains 137 mM NaCl, 2.7 mM KCl, 8 mM $Na_2HPO_4$, and 2 mM $KH_2PO_4$) or SFN (50 mg/kg) in PBS by intraperitoneal injection every Monday, Wednesday, and Friday for 3 months, beginning 1 month after the AAV1-Rz-SOD2 injection.

*Visual function test:* Visual function was assessed with electroretinography (ERG) performed at pretreatment as baseline, 1 month after AAV1-Rz-SOD2 injection, and 4 months after AAV1-Rz-SOD2 injection as previously described [33]. For the ERGs, the mice were dark-adapted overnight, and full-field ERGs were recorded with a visual electrodiagnostic system (UTAS-E 2000; LKC Technologies, Gaithersburg, MD) using gold wire loop electrodes placed on each cornea and a reference electrode placed subcutaneously between the eyes. Scotopic rod recordings were performed with stimuli presented at intensities of 0.025, 0.25, and 2.5 log cd-s/$m^2$ at 10-, 20-, and 30-s intervals, respectively. Ten responses were recorded and averaged at each light intensity. Photopic cone recordings were performed after the mice were light adapted to a white background light of 100 cds/$m^2$ for 5 min. Recordings were performed with four-increasing flash intensities from 0, 5, 10, and 25 log cd-s/$m^2$ in the presence of a constant 100 mcds/$m^2$ rod suppressing background light. Fifty responses were recorded and averaged at each intensity. The a-waves were measured from the baseline to the peak in the negative direction, and the b-waves were measured from the negative peak to the major positive peak. The ERG data are presented as comparisons between treatment conditions for the mean of the maxima for a- and b-wave responses.

*SD-OCT imaging:* Eyes were dilated with 1% atropine, followed by 2.5% phenylephrine hydrochloride (Alcon, Fort Worth, TX), and then mice were anesthetized with ketamine (72 mg/kg)/xylazine (4 mg/kg). One drop of 2.5% hydroxypropyl methylcellulose (Gonak; Akorn, Lake Forest, IL) was applied to each eye before examination. Spectral domain optical coherence tomography (SD-OCT) was performed using the InVivoVue OCT system (Bioptigen, Inc., Durham, NC). Three lateral images (nasal, central, and temporal) were collected, starting 0.2 mm above the meridian crossing through the center of the optic nerve (ON), at the ON meridian, and 0.2 mm below the ON meridian. A corresponding box centered on the ON with eight measurement points separated by 0.2 mm from each other was created. Corresponding neural retinas from different treatments were compared at the same location (0.2 mm temporal to the ON) from the vitreous face of the ganglion cell layer to the apical face of the RPE across the retina.

*Histopathology and immunohistochemical analyses:* Eyes were enucleated, immediately fixed in 4% paraformaldehyde overnight at 4 °C, and embedded in paraffin. Five-micron sections were prepared. For routine histology, sections were stained with hematoxylin and eosin (H&E) according to standard protocols by the UAB Pathology Core. The stained sections were evaluated by microscopy and photographed.

For immunohistochemistry, the sections were deparaffinized and processed for antigen-epitope retrieval. Samples were incubated in a steamer (Histofine, Nichirei Biosciences Inc., Tokyo, Japan) at 120 °C for 30 min in antigen retrieval solution and rodent deblocker (Biocare Medical) for antigen retrieval and then allowed to cool. The sections were permeabilized with 0.3% Triton X-100 for 10 min and then blocked with 5% normal goat sera, plus 1% bovine serum albumin (BSA) for 1 h at room temperature and incubated with rabbit anti-IBa1 (1:400 in blocking solution) or rat anti-F4/80 (1:200) overnight at 4 °C. The sections were then incubated with Alexa Fluor 594 goat anti-rabbit immunoglobulin G (IgG) or Alexa Fluor 488 goat anti-rat (1:600 in blocking solution; Invitrogen) for 1 h at room temperature. After extensive washing with PBS, the sections were mounted with Vectashield

4',6-diamidino-2-phenylindole (DAPI; Vector Laboratories) for nuclear staining. Negative control samples were processed with omission of the primary antibody. The sections were examined using an Axio Vert 135 fluorescence microscope (Carl Zeiss, Thornwood, NY) with identical settings for laser intensity, gain, etc.

For MnSOD immunohistochemistry, the sections were deparaffinized and processed for antigen-epitope retrieval at 95–100 °C for 10 min in R-Universal Epitope Recovery Buffer Electron Microscopy Sciences, Hatfield, PA and then allowed to cool. The sections were blocked with 10% normal donkey sera plus 3% BSA for 1 h at room temperature and incubated with rabbit anti-MnSOD (ProteinTech, Rosemont, IL, cat# 24,127-1-AP, 1:1,000 in blocking solution) overnight at 4 °C. The sections were then incubated with Alexa Fluor 546 donkey anti-rabbit IgG (1:400 in blocking solution; Invitrogen) plus Hoechst 33342 (Molecular Probes Eugene, OR) for 1 h at room temperature. After extensive washing with PBS, the sections were mounted with ProLong Gold (ThermoFisher Scientific, Waltham, MA). Negative control samples were processed with omission of the primary antibody. The sections were examined using a Nikon TE2000 (Tokyo, Japan) as previously described [50]. MnSOD labeling of the RPE layer and photoreceptor inner segments was quantified from images using ImageJ. Those involved in the experiments were masked to the treatments.

*Statistical analysis:* The results are expressed as mean ± standard error of the mean (SEM). All experiments were assessed by comparing two group mean values using an unpaired Student *t* test. Comparisons of different treatments between more than two groups were assessed using one-way ANOVA with Bonferroni post hoc tests to determine the significance of the results in all assays and functional tests. All analyses were performed using Prism 5 ver. 5.01 (GraphPad Software, Inc., La Jolla, CA). A p value of less than 0.05 considered statistically significant.

## RESULTS

To test whether the efficacy of SFN to mitigate retinal degeneration requires Nrf2, we performed the study outlined in Figure 1. Six- to 8-month-old, strain-matched wild-type (WT) and global Nrf2 KO mice in a C57BL/6J background negative for the *Rd8* mutation were subjected to baseline ERG and OCT measurements. The animals were then injected subretinally with AAV1-RzSOD2, an adeno-associated virus (AAV) expressing a ribozyme targeting superoxide dismutase 2 (SOD2) mRNA to induce oxidative stress in the RPE [31-33]. The contralateral eye of each animal was not injected. One month after the subretinal injections, ERG and OCT measurements were recorded again. The mice were subsequently administered 50 mg/kg of SFN (or PBS vehicle) by intraperitoneal injection three times per week (Monday, Wednesday, and Friday) for 3 months. Final ERG and OCT measurements were recorded before the mice were euthanized. Mice were euthanized by intraperitoneal injection of xylazine and ketamine (2.5 and 17.5 mg/kg body weight respectively), followed by the cervical dislocation. Postmortem histology of the posterior eye was performed using H&E staining to evaluate the retinal morphology and specific antibodies to detect markers of inflammation. The mice were 10–12 months of age at study completion. In keeping with convention, we use the term "SOD2" when referring to the gene and mRNA species and "MnSOD" when referring to the enzyme.

A comparison of the ERG profiles from the 6- to 8-month-old mice before MnSOD knockdown revealed that relative to the untreated WT mice, the Nrf2 KO mice had modestly decreased scotopic a- and b-waves (Figure 2A,B, respectively), a phenotype previously observed in mice lacking this transcription factor [46], whereas photopic b-waves were comparable between genotypes (Figure 2C). Although there were no significant ERG differences detected between the left (OS) and right (OD) eyes of the WT mice (Figure 2D–F), the Nrf2 KO animals curiously displayed modestly reduced scotopic a-waves in the OS compared to OD eyes (Figure 2D). AAV1-RzSOD2-mediated knockdown (KD) of MnSOD enzyme expression induced a significant reduction in all ERG waves for the WT and Nrf2 KO mice 1 month after ribozyme subretinal injection (Figure 2G–I). The extent of the ERG decreases was comparable between genotypes (Figure 2G–I), indicating that the absence of Nrf2 did not amplify the functional consequences of MnSOD suppression in the RPE. Three months of SFN treatment conferred no significant improvement on the scotopic a- and b-waves in the SOD2 kDa eyes for either the WT or Nrf2 KO mice (Figure 2J–K) but significantly improved the photopic b-waves in the WT-SOD2 kDa eyes (Figure 2L). This photopic b-wave recovery required Nrf2 expression, as a comparable improvement in cone function did not occur in the Nrf2KO-RzSOD2-SFN mice (Figure 2L).

In parallel with the longitudinal ERG measurements, SD-OCT was performed to track morphological integrity in vivo. Comparing untreated 6- to 8-month-old WT and Nrf2 KO mice before any treatments, we did not observe significant differences in retinal thickness between genotypes (Figure 3A) or between left and right eyes within a genotype (Figure 3B). However, we observed modest RPE disruptions in a subset of Nrf2 KO mice (Figure 3C versus 3D, arrows).

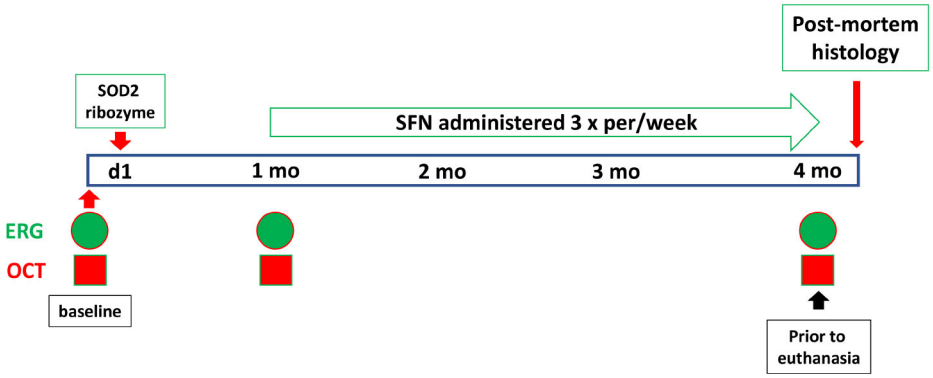


Figure 1. Study schematic. Baseline electroretinography (ERG) and OCT measurements from 6- to 8-month-old WT and Nrf2 KO mice were recorded before any interventions, and the animals were subsequently injected subretinally with AAV1-RzSOD2 to knock down MnSOD enzyme expression in the RPE layer of the right eyes (OD). The contralateral eye (OS) was untreated. One month later, ERG and OCT measurements were taken again, and the mice were administered sulforaphane (50 mg/kg) or vehicle every Monday, Wednesday, and Friday for 3 months. Mice were 10–12 months old at the end of the study. Final ERG and OCT measurements were recorded before postmortem harvesting of the posterior eyes for histopathology and immunohistochemistry.

One month after ribozyme-mediated SOD2 mRNA KD, we observed the expected retinal thinning in the WT and Nrf2 KO mice (Figure 3E), and this thinning was exacerbated by 12% in the Nrf2 KO animals. Three months of SFN treatment conferred no significant protection on MnSOD KD retinas in the WT animals (Figure 3F). In contrast, SFN modestly recovered the retinal thickness in the Nrf2 KO-MnSOD KD retinas (Figure 3F). Similarly, SFN improved the retinal thickness in the uninjected eyes of the Nrf2 KO animals, with statistics bordering on significance (Figure 3F, p=0.051).

Complementary postmortem histological analyses of retinas from 10- to 12-month-old mice were performed on four sets of mice for each genotype [1]: untreated [2], SFN treatment in the absence of MnSOD KD [3], vehicle treatment following MnSOD KD, and [4] SFN treatment following MnSOD KD. Analysis of the untreated eyes revealed comparable retinal morphology (Figure 4A, top and bottom panels). The WT and Nrf2 KO mice treated with SFN in the absence of MnSOD KD had mild morphological defects (Figure 4B). Specifically, in the WT mice, the RPE layer consistently showed patchy areas of atrophy (Figure 4B, top panels, red arrows), whereas the RPE layers in some Nrf2 KO mice contained vacuoles (Figure 4B, bottom panel, red arrows). The WT mice subjected to MnSOD KD and treated with vehicle displayed gross disorganization of the neural retina, retinal thinning, severe atrophy of the RPE layer, and the presence of subretinal cellular infiltrates likely representing infiltrating inflammatory cells (Figure 4C, top panel). Likewise, the Nrf2 KO mice subjected to MnSOD KD and treated with vehicle exhibited highly disorganized neural retina morphology, severe retinal thinning and RPE atrophy, and extensive subretinal infiltrates accompanied by fibrosis (Figure 4C, bottom panel, red arrows). Treatment of the WT mice with SFN following MnSOD KD improved the morphology of the retina and the RPE compared to vehicle treatment, although the morphology was not comparable to baseline levels (Figure 4D, top panel). Similarly, SFN partially preserved the retinal and RPE morphology in the Nrf2 KO mice administered SFN after MnSOD KD, although RPE atrophy, infiltrates, and fibrosis were still detectable (Figure 4D, bottom panel).

Transverse retinal sections were labeled for the inflammatory markers Iba1 and F4/80. Iba1 staining was minimal in untreated animals but significantly increased in both genotypes after MnSOD KD, with increased numbers of ramified microglia in the inner retina and subretinal space (Figure 5A). This was markedly reduced in the MnSOD KD mice following SFN treatment. Staining for the macrophage marker F4/80 revealed a similar profile with maximum staining confirming macrophage infiltration in the WT and Nrf2 KO-MnSOD KD mice, which was reduced by SFN treatment (Figure 5B).

## DISCUSSION

This study tested the capacity of SFN to restore retinal integrity and function in mice following oxidative stress–induced damage to the RPE layer induced by the ribozyme-mediated knockdown of MnSOD in the RPE. This model increases mitochondrial superoxide levels, which yield dAMD-like pathologies [31-35]. SFN treatment was initiated 1 month after delivery of an SOD2-targeting ribozyme to evaluate the interventional utility of this phytochemical during active disease and to complement previous studies testing the prophylactic efficacy of the compound (e.g., [51-53]). SFN was administered three times a week for 3 months such that

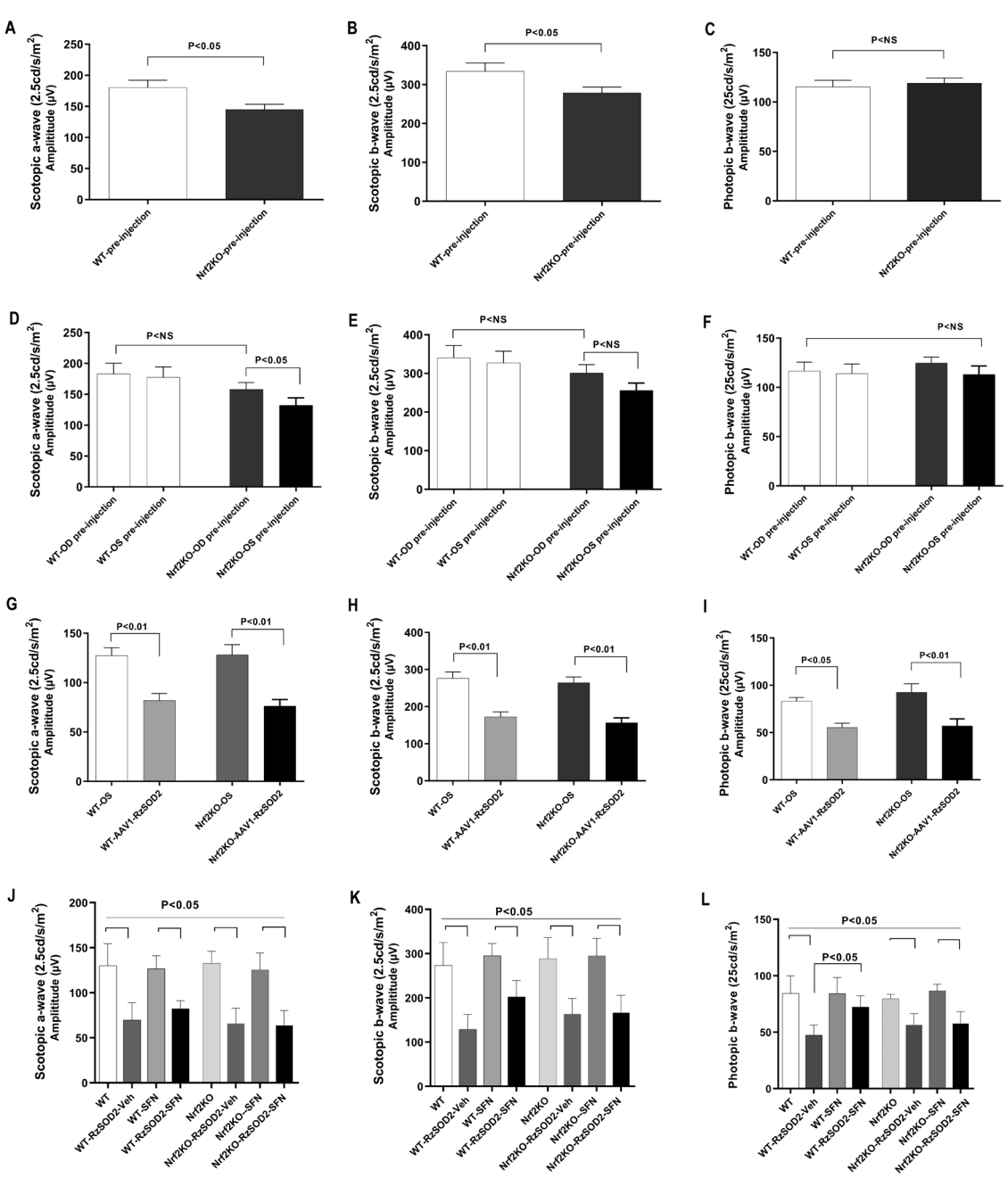


Figure 2. SFN improves the photopic b-wave ERG deficit induced by MnSOD knockdown in an Nrf2-dependent manner. Full-field scotopic and photopic electroretinography (ERG) were performed on WT and Nrf2 KO mice. Error bars represent SEM (standard error of the mean). **A**–**C**: Graphs show baseline scotopic a-waves, scotopic b-waves, and photopic b-waves, respectively, for each genotype with data from both eyes combined. **D**–**F**: Graphs of baseline scotopic a-waves, scotopic b-waves, and photopic b-waves, respectively, for each genotype from the right (OD) and left (OS) eyes. **G**–**I**: All mice were injected with AAV1-RzSOD2 in the OD, and 1 month post-AAV administration, ERGs were recorded. **J**–**L**: One month post-AAV administration, mice from each genotype were evenly divided into two groups and treated with either vehicle (Veh) or SFN. After 3 months of treatment (i.e., 4 months post-AAV administration), a final set of ERGs were recorded for each animal. Statistical significance ($p<0.05$) was determined with an unpaired Student *t* test or one-way ANOVA using GraphPad Prism.

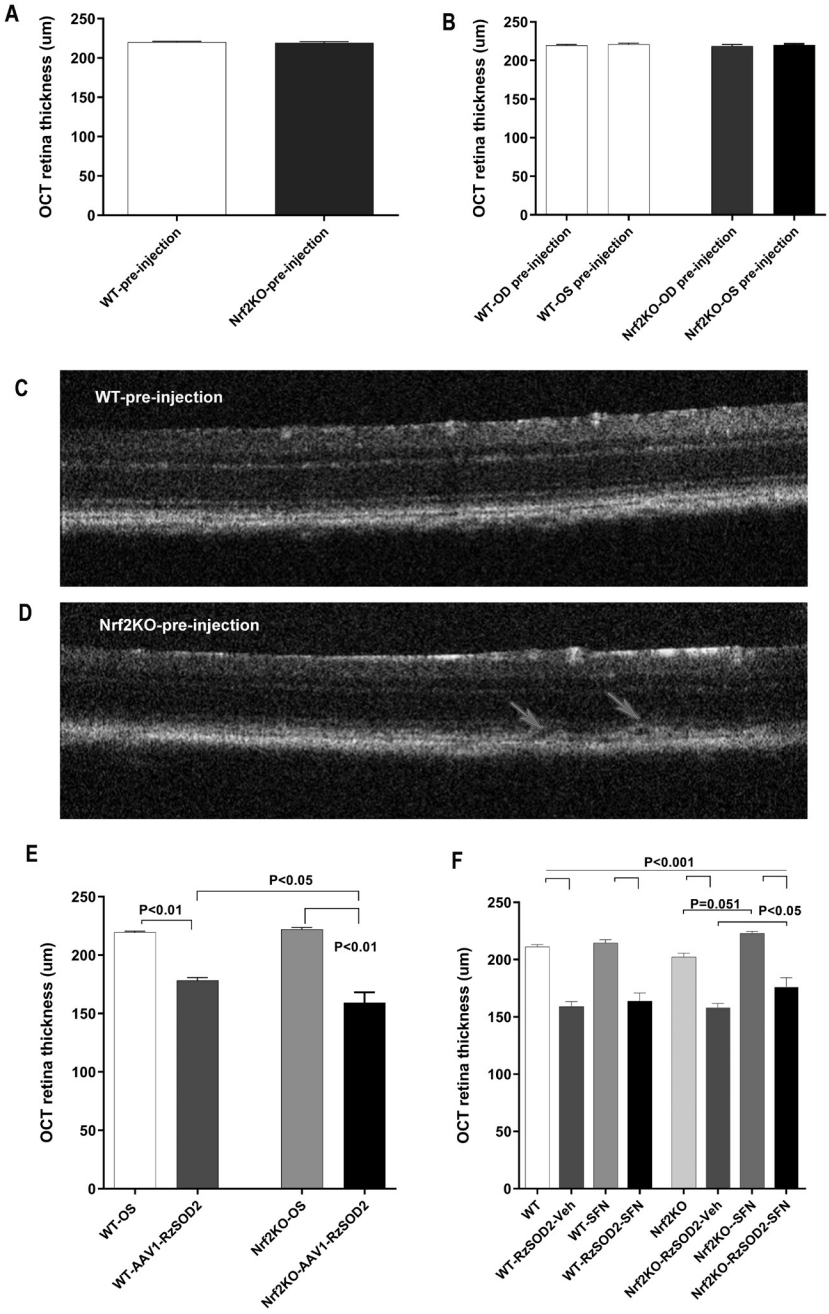


Figure 3. MnSOD knockdown decreases retinal thickness as measured with OCT, and SFN improves retinal thickness in Nrf2 KO mice. **A**–**B**: spectral domain-optical coherence tomography (SD-OCT) was used to measure and compare retinal thickness in the eyes of WT and Nrf2 KO mice before any treatments. Error bars represent SEM (standard error of the mean). Representative SD-OCT images of WT (**C**) and Nrf2 KO (**D**) eyes before subretinal injections. Arrows in (**D**) denote disruptions to the RPE layer observed in a subset of Nrf2 KO mice before the AAV1-RzSOD2 injection. Graphs of SD-OCT measurements taken 1 month (**E**) and 4 months (**F**) after AAV1-RzSOD2 delivery (i.e., 3 months after SFN treatment was initiated). Statistical significance ($p<0.05$) was determined with an unpaired Student *t* test or one-way ANOVA using GraphPad Prism.

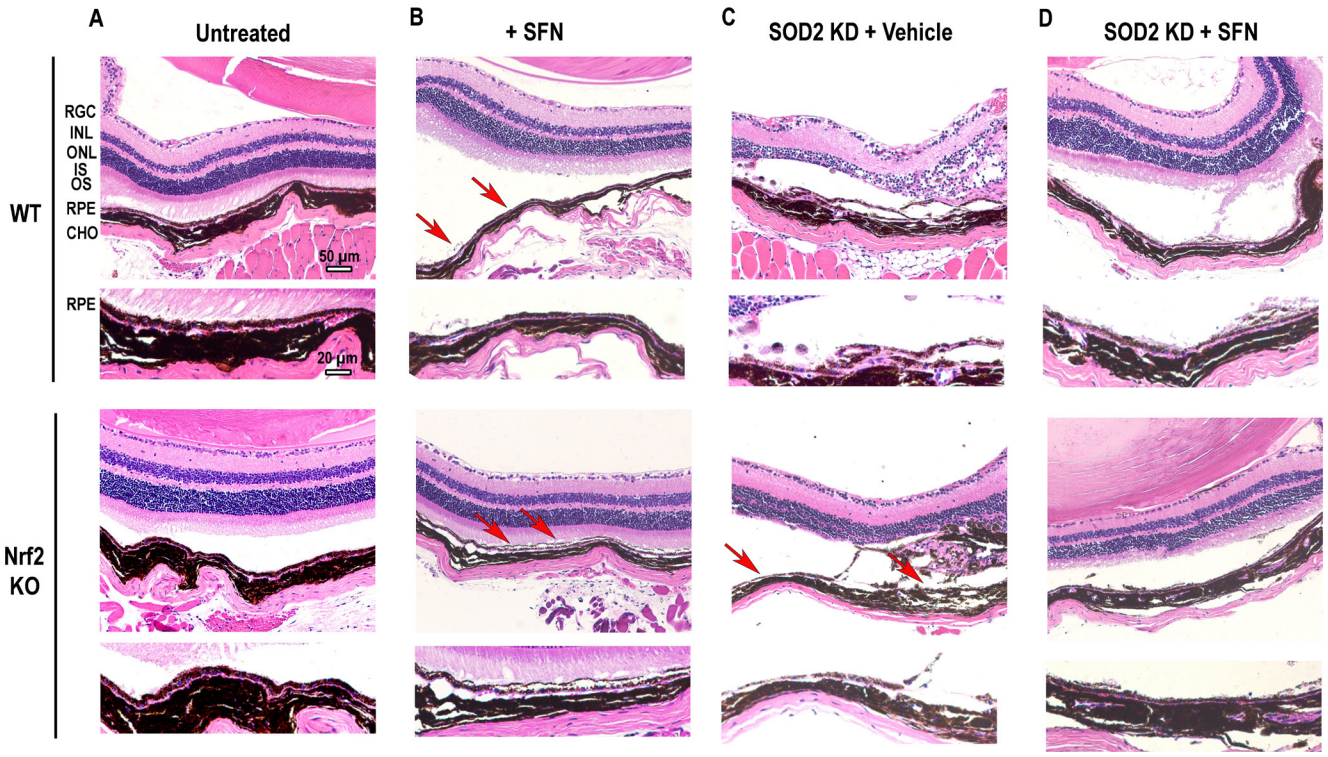


Figure 4. SFN treatment can restore the retinal morphology disrupted by MnSOD knockdown. Postmortem histological sections (5 m thick) of retinas prepared from WT and Nrf2 KO mice and labeled with hematoxylin and eosin (H&E) staining. The images in the top row are from WT eyes, and the images in the bottom row are from Nrf2 KO eyes. Sections were prepared from animals: (**A**) untreated, (**B**) treated with SFN in the absence of MnSOD knockdown, (**C**) administered AAV1-RzSOD2 to knock down MnSOD, and (**D**) administered AAV1-RzSOD2 to knock down MnSOD and treated with SFN. Red arrows in (**B**) mark patchy areas of atrophy (top panel) and subretinal vacuoles (bottom panel). In the bottom panel of (**C**), red arrows denote severe retinal/RPE thinning and subretinal infiltrates.

the study was terminated 4 months after ribozyme injection, a time point at which AMD-like structural and functional pathologies from MnSOD knockdown are readily detectable [31]. This study further compared the efficacy of SFN in WT mice versus Nrf2 KO mice, as SFN activates Nrf2, but age-dependent reductions of Nrf2 in the RPE [28,29] and other cell types (e.g., [30]) may limit the clinical feasibility of exploiting Nrf2 activation in elderly patients.

SFN restored the ERG photopic b-wave deficit induced by MnSOD loss in a Nrf2-dependent manner (Figure 2L), consistent with unchecked oxidative stress within the RPE causing functional deficiencies in photoreceptor cones (e.g., [34,35]) and Nrf2 target gene products neutralizing this stress sufficiently to recover cone function [54,55]. This functional rescue is promising, as cone loss associated with oxidative stress is characteristic of AMD [56,57] and retinitis pigmentosa (RP) [58]. In contrast, SFN did not recover rod function (Figure 2J,K). Cones are likely more vulnerable to oxidative damage than rods due to the higher mitochondrial content [58] and higher sensitivity to the mitochondrial toxin, $FeSO_4$ (e.g., [59]). The elevated mitochondrial content of cones may be accompanied by a more robust antioxidant capacity to neutralize endogenous free radicals generated by mitochondrial respiration, conferring on cones higher resistance to oxidative stress originating in neighboring RPE cells and rods. The differential sensitivity between rods and cones to exogenous stresses has been observed in diabetic mice; rod a- and b-wave ERGs decreased by 50%, whereas cone a- and b-wave ERGs were not deleteriously impacted [60]. In addition, Nrf2 overexpression selectively rescued cones in several mouse models of retinal degeneration (rd) [55], as did antioxidant supplementation [61], and greater functional rescue of cones by SFN has been reported for the rd10 model of RP [62].

Rod photoreceptors may incur irreparable damage from chronic oxidative stress, consistent with scotopic ERG deficits in untreated Nrf2 KO mice (Figure 2A,B), whereas cone photopic ERGs were comparable between genotypes (Figure 2C). Zhao et al. reported a selective reduction in rod function in mice genetically ablated for Nrf2 [46]. The

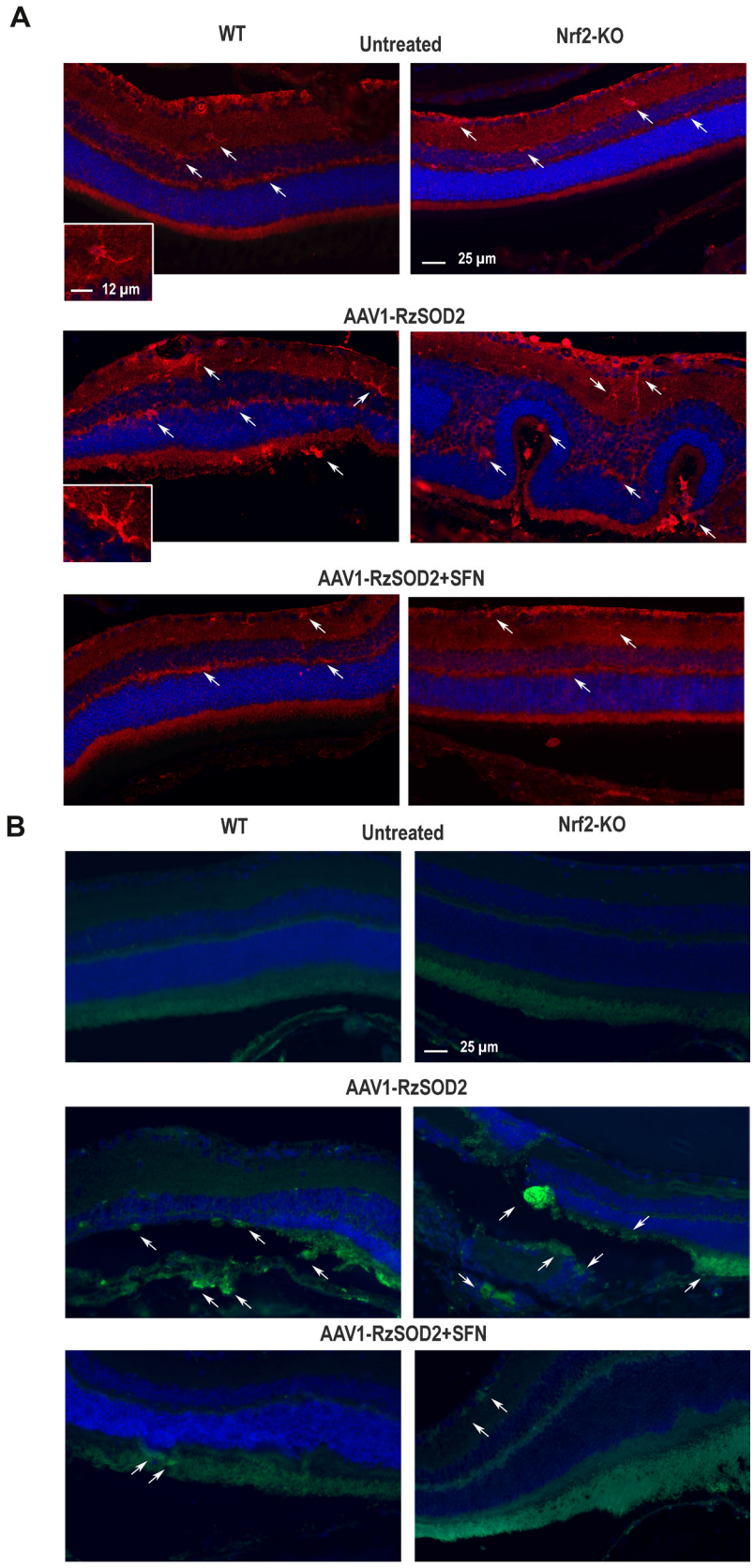


Figure 5. SFN treatment reduces microglia and macrophage infiltration in SOD2 knockdown mice. Representative transverse sections of retinas from wild type (WT) and Nrf2 KO mice either untreated, MnSOD KD or MnSOD KD plus SFN treatment. **A**: Immunostaining for the microglia marker IBA1 (red) shows increased microglia and ramification in the retinas of the MnSOD KD animals and reduction after SFN treatment. **B**: Immunostaining for the macrophage marker F4/80 (green) shows increased infiltration in the retina following MnSOD KD and reduction after SFN treatment.

higher susceptibility of rods to Nrf2 loss could also stem from differences in rods and cones with respect to fatty acid compositions [63], metabolic and bioenergetic requirements [39], and autophagic capacity [58,64-66]. Nrf2 activity is required for efficient autophagy and lysosomal function in the RPE [46], and SFN protects RPE cells from blue light–induced inflammation and apoptosis by inducing autophagy [67]. These findings, along with reports that SFN can either induce or inhibit autophagy depending on the cell type and experimental conditions (e.g., [68,69]), highlight an important future direction to determine the extent by which SFN differentially impacts the autophagic machinery in rods versus cones. The balance between autophagy and proteasomal degradation in photoreceptors governs the capacity of these cells to retain function in response to stress (e.g., [70]). As SFN can increase lysosomal and mitochondrial biogenesis (e.g., [68,71-73], we favor that the benefit to cones stems from SFN concomitantly increasing the removal of damaged mitochondria by mitophagy while inducing the biogenesis of replacement mitochondria.

SFN mitigates retinal degeneration in rodent models of ischemia/reperfusion [51,74,75], light damage [52,53], genetic models [62,76], and diabetes [60,77,78]. The compound improves ERGs [52,53,62,74,76,78], reduced retinal thinning [74,75], and suppressed proinflammatory cytokines [51,77]. These positive effects have been consistently reported and include studies that initiated SFN treatment before the onset of pathologies (e.g., [51-53]. In this context, SFN preserves rod ERG function when administered before light-induced retinal damage [52,53], implying that protecting rods depends on mitigating the initial (photo)oxidative insult before damage.

Despite failing to recover rod function in Nrf2 knockout mice with MnSOD knockdown, SFN modestly increased retinal thickness in these mice (Figure 3F) and improved the morphological markers of RPE atrophy and retinal degeneration in both genotypes (Figure 4D). However, these improvements did not correlate proportionally with functional recovery in either genotype. Incomplete morphological and functional rescue has been observed with other therapeutic interventions (e.g., [79,80]), likely reflecting irreparable damage of photoreceptors during the first month of MnSOD knockdown before SFN treatment. Further protection may be achievable if SFN treatment is initiated simultaneously with ribozyme delivery.

This study has potential caveats and limitations. First, control mice injected with an AAV-inactive ribozyme were not included due to the limited number of Nrf2 KO animals available because of breeding issues and reduced litter sizes. Second, MnSOD expression can be induced as a direct Nrf2 target gene product, as most convincingly demonstrated by the Nrf2 antibody chromatin immunoprecipitation (CHIP) approach in cells treated with astragaloside [81]. Constitutive MnSOD expression, however, is independent of Nrf2 (e.g., [82]). Numerous other transcription factors regulate MnSOD expression, including NF-kB, specificity protein 1 (SP1), AP-2, and C/EBP (reviewed in [83], raising the possibility that the efficacy of SFN in wild-type mice results from Nrf2-mediated transcription of SOD2 mRNA that counters the efficiency of the ribozyme. However, the evidence does not favor this scenario because the activity of the ribozyme was not detectable during the time period that SFN was administered, as indicated by a plateauing of the ERG deficits between the first and fourth months after ribozyme delivery in vehicle-treated mice, irrespective of genotype (Appendix 1). Moreover, labeling of the RPE in paraffin sections with an MnSOD antibody did not show a detectable change in enzyme expression in response to SFN compared to RPE cells from vehicle-treated eyes (Appendix 1). As SFN treatment was not initiated until 1 month after ribozyme administration when the ERG deficits plateaued, the improved photopic ERG readings in the WT mice are more consistent with the compound restoring cone function independent of replenishing MnSOD expression in the RPE.

An additional consideration is that the SOD2 mRNA knockdown is targeted to the RPE layer, but SFN was delivered systemically. Thus, the impacts of SFN are not restricted to the RPE; however, the individual relative contributions of each cell type (e.g., RPE, photoreceptors, or Mller cells) to the overall efficacy of SFN are unknown. These relative contributions depend on [1] the expression levels of Nrf2 and other factors activated or inhibited by SFN (e.g., histone deacetylases) [2, 7-12], the susceptibility and responses of each cell type to oxidative stress and mitochondrial dysfunction, and [3] the metabolic flexibility and bioenergetic needs of each cell type. Notably, the MnSOD levels in the inner segments of photoreceptors were not detectably changed by SFN in the WT mice but trended higher in the Nrf2 KO mouse inner segments (Appendix 1). However, functional rescue was observed only in the WT animals, indicating that MnSOD induction in photoreceptors is not likely a major contributor to SFN efficacy in this study.

Extrapolating the in vivo impacts of SFN on the mouse retina to human AMD is complicated by the lack of a macula in rodents. Thus, whether SFN exerts similar protective effects on cones in the macula or fovea cannot be inferred from these studies. Further, because the photoreceptor subpopulations in this specialized region of the primate retina may have distinct physiologic and bioenergetic requirements

[39], the impacts of SFN on each of these cell types may differ from the response of photoreceptors in the peripheral retina of humans or in the mouse retina. The relative levels of Nrf2 transcriptional activity in photoreceptor subpopulations within and surrounding the macula during health and disease is currently unknown, but would be valuable for determining the therapeutic potential of manipulating Nrf2 to ameliorate retinal degeneration [54,55]. An additional caveat is that this study utilizes a genetic knockout model of Nrf2, whereas only a partial Nrf2 deficiency has been reported in human RPE [28]. Therefore, SFN may confer some benefit on cone function for humans retaining partial Nrf2 transcriptional activity in the RPE.

Moving forward, it will be important to determine which cell types mediate SFN efficacy, as well as the mechanisms conferring neuroprotection. We speculate that these findings reflect the differential responses of rods and cones to reduced ATP production by mitochondria in the RPE layer. Genetic ablation of Nrf2 and knockdown of MnSOD compromise mitochondrial integrity and ATP generation [34,41,84]. The suppression of mitochondrial respiration in RPE cells deleteriously impacts photoreceptor survival and function [38], as RPE cells utilize oxidative phosphorylation to spare glucose for photoreceptors (e.g., [34,37,85-87]). Suppressed ATP production by RPE mitochondria induces a cellular switch to glycolysis, thus reducing glucose availability for photoreceptors, as documented in the RPE [34] and muscle [41] following SOD2 gene ablation. Limiting glucose oxidation by photoreceptors further reduces lactate production and secretion for use by the RPE and Müller glia resulting in disrupted bioenergetic homeostasis across the posterior eye (reviewed in [37,85]). Glucose starvation of photoreceptors may adversely affect rods disproportionately compared to cones, as rods have a higher reliance on glycolytic metabolism [88-90] but contain lower glycogen stores than cones [90]. This may account for the preferential restoration of cone function by SFN (Figure 2). Reduced mitochondrial respiration in RPE cells also decreases oxygen consumption, resulting in a local hyperoxia that can be toxic to photoreceptors [91-93].

ATP deficits and mitochondrial dysfunction in RPE cells impact the mammalian target of rapamycin (mTOR) kinase complexes (mTORC1 and mTORC2), which integrate nutrient availability with bioenergetics, protein synthesis, and proliferation (reviewed in [94]). RPE mTOR activity is mediated by ATP levels as well as by mitochondrial (dys)function (e.g., [95,96]), and chronic mTOR signaling in the RPE causes dedifferentiation, leading to photoreceptor and choroid degeneration [96-98]. However, SFN induces mitochondrial biogenesis [71,99,100], a cellular response accompanied by enhanced mTOR activity that may underlie the neuroprotection conferred by the compound [101]. Notably, enhanced mTOR activity protects cones in mouse models of RP [102,103]. Thus, the efficacy of SFN given every other day in the present study could involve periodic elevations of mTOR activity in cones. Additional factors contributing to the efficacy of SFN may involve Nrf2-mediated induction of the rate-limiting enzymes for numerous bioenergetic pathways (e.g., the pentose phosphate pathway, the polyol pathway, the hexosamine pathway, the β-oxidation of fatty acids, or other intermediary pathways of metabolism) [18,84,104].

In conclusion, the findings of this study underscore that SFN has efficacy in maintaining retinal function and morphological integrity but likely requires optimization of the timing of administration and dosing frequency [2], preserves cone function in a Nrf2-dependent manner, and [3] may optimally be used as an adjuvant treatment with other therapies that enhance photoreceptor function. These findings highlight the therapeutic value of SFN and the potential limitations of the compound in ocular cells with compromised Nrf2 activity.

## APPENDIX 1. ERG DEFICITS ARE COMPARABLE 1 MONTH AND 4 MONTHS AFTER SUB-RETINAL INJECTION OF AN SOD2-TARGETING RIBOZYME.

To access the data, click or select the words "Appendix 1." Longitudinal analysis of ERG amplitudes in WT and Nrf2 KO mouse eyes comparing measurements taken 1 month and 4 months post AAV1-RzSOD2 injection. The ERG differences between the two time points were not statistically significant in either genotype for the scotopic a-wave (**A**), the scotopic b-wave (**B**), or the photopic b-wave (**C**). All comparisons represent mean + SEM, $p>0.05$ using *t* test and one-way ANOVA $n\geq6$ mice per genotype per treatment. (**D**) Representative photomicrographs taken with a 60× objective of RPE sections labeled with an MnSOD antibody from WT and Nrf2 KO eyes that have not (-Rz) or have (+Rz) been injected with a ribozyme targeting MnSOD expression. Mice were treated with vehicle (Veh) or SFN (SFN). Graph compiled from 3 independent sections quantified for each experimental condition. No statistically significant differences (ns) were detected between MnSOD levels using Student *t* test. (E) Representative photomicrographs taken with a 20× objective of retinal sections labeled with an MnSOD antibody, as in (D). MnSOD expression in the inner segments of Nrf2 KO mice compared to WT mice trended toward but did not reach statistical significance (ns) using Student *t* test.

## ACKNOWLEDGMENTS

This work was supported by National Institutes of Health Grant R01EY024944 (to SMP), grant HR16–068 from The Oklahoma Center for the Advancement of Science and Technology (to SMP), and a grant from the Presbyterian Health Foundation (to SMP). We are grateful to members of the Plafker and Boulton laboratories for helpful discussions.

## REFERENCES

1. Yang L, Palliyaguru DL, Kensler TW. Frugal chemoprevention: targeting Nrf2 with foods rich in sulforaphane. Semin Oncol 2016; 43:146-53. [PMID: 26970133].
2. Shapiro TA, Fahey JW, Wade KL, Stephenson KK, Talalay P. Human metabolism and excretion of cancer chemoprotective glucosinolates and isothiocyanates of cruciferous vegetables. Cancer Epidemiol Biomarkers Prev 1998; 7:1091-100. [PMID: 9865427].
3. Tian S, Liu X, Lei P, Zhang X, Shan Y. Microbiota: a mediator to transform glucosinolate precursors in cruciferous vegetables to the active isothiocyanates. J Sci Food Agric 2018; 98:1255-60. [PMID: 28869285].
4. Zhang Y, Talalay P, Cho CG, Posner GH. A major inducer of anticarcinogenic protective enzymes from broccoli: isolation and elucidation of structure. Proc Natl Acad Sci USA 1992; 89:2399-403. [PMID: 1549603].
5. Mangla B, Javed S, Sultan MH, Kumar P, Kohli K, Najmi A, Alhazmi HA, Al Bratty M, Ahsan W. Sulforaphane: A review of its therapeutic potentials, advances in its nanodelivery, recent patents, and clinical trials. Phytother Res 2021; .
6. Yagishita Y, Fahey JW, Dinkova-Kostova AT, Kensler TW. Broccoli or Sulforaphane: Is It the Source or Dose That Matters? Molecules 2019; 24:3593-631. [PMID: 31590459].
7. Myzak MC, Dashwood RH. Chemoprotection by sulforaphane: keep one eye beyond Keap1. Cancer Lett 2006; 233:208-18. [PMID: 16520150].
8. Myzak MC, Dashwood WM, Orner GA, Ho E, Dashwood RH. Sulforaphane inhibits histone deacetylase in vivo and suppresses tumorigenesis in Apc-minus mice. FASEB J 2006; 20:506-8. [PMID: 16407454].
9. Myzak MC, Hardin K, Wang R, Dashwood RH, Ho E. Sulforaphane inhibits histone deacetylase activity in BPH-1, LnCaP and PC-3 prostate epithelial cells. Carcinogenesis 2006; 27:811-9. [PMID: 16280330].
10. Myzak MC, Ho E, Dashwood RH. Dietary agents as histone deacetylase inhibitors. Mol Carcinog 2006; 45:443-6. [PMID: 16652377].
11. Myzak MC, Karplus PA, Chung FL, Dashwood RH. A novel mechanism of chemoprotection by sulforaphane: inhibition of histone deacetylase. Cancer Res 2004; 64:5767-74. [PMID: 15313918].
12. Myzak MC, Tong P, Dashwood WM, Dashwood RH, Ho E. Sulforaphane retards the growth of human PC-3 xenografts and inhibits HDAC activity in human subjects. Exp Biol Med (Maywood) 2007; 232:227-34. [PMID: 17259330].
13. O'Mealey GB, Berry WL, Plafker SM. Sulforaphane is a Nrf2-independent inhibitor of mitochondrial fission. Redox Biol 2017; 11:103-10. [PMID: 27889639].
14. Maheo K, Morel F, Langouet S, Kramer H, Le Ferrec E, Ketterer B, Guillouzo A. Inhibition of cytochromes P-450 and induction of glutathione S-transferases by sulforaphane in primary human and rat hepatocytes. Cancer Res 1997; 57:3649-52. [PMID: 9288764].
15. Bonnesen C, Eggleston IM, Hayes JD. Dietary indoles and isothiocyanates that are generated from cruciferous vegetables can both stimulate apoptosis and confer protection against DNA damage in human colon cell lines. Cancer Res 2001; 61:6120-30. [PMID: 11507062].
16. Fimognari C, Nusse M, Berti F, Iori R, Cantelli-Forti G, Hrelia P. Cyclin D3 and p53 mediate sulforaphane-induced cell cycle delay and apoptosis in non-transformed human T lymphocytes. Cell Mol Life Sci 2002; 59:2004-12. [PMID: 12530531].
17. Gamet-Payrastre L, Li P, Lumeau S, Cassar G, Dupont MA, Chevolleau S, Gasc N, Tulliez J, Terce F. Sulforaphane, a naturally occurring isothiocyanate, induces cell cycle arrest and apoptosis in HT29 human colon cancer cells. Cancer Res 2000; 60:1426-33. [PMID: 10728709].
18. Hayes JD, Dinkova-Kostova AT. The Nrf2 regulatory network provides an interface between redox and intermediary metabolism. Trends Biochem Sci 2014; 39:199-218. [PMID: 24647116].
19. Dinkova-Kostova AT, Holtzclaw WD, Cole RN, Itoh K, Wakabayashi N, Katoh Y, Yamamoto M, Talalay P. Direct evidence that sulfhydryl groups of Keap1 are the sensors regulating induction of phase 2 enzymes that protect against carcinogens and oxidants. Proc Natl Acad Sci USA 2002; 99:11908-13. [PMID: 12193649].
20. Hu C, Eggler AL, Mesecar AD, van Breemen RB. Modification of keap1 cysteine residues by sulforaphane. Chem Res Toxicol 2011; 24:515-21. [PMID: 21391649].
21. Itoh K, Wakabayashi N, Katoh Y, Ishii T, Igarashi K, Engel JD, Yamamoto M. Keap1 represses nuclear activation of antioxidant responsive elements by Nrf2 through binding to the amino-terminal Neh2 domain. Genes Dev 1999; 13:76-86. [PMID: 9887101].
22. McMahon M, Lamont DJ, Beattie KA, Hayes JD. Keap1 perceives stress via three sensors for the endogenous signaling molecules nitric oxide, zinc, and alkenals. Proc Natl Acad Sci USA 2010; 107:18838-43. [PMID: 20956331].
23. Zhang DD, Hannink M. Distinct cysteine residues in Keap1 are required for Keap1-dependent ubiquitination of Nrf2 and for stabilization of Nrf2 by chemopreventive agents and oxidative stress. Mol Cell Biol 2003; 23:8137-51. [PMID: 14585973].
24. Zhang DD, Lo SC, Cross JV, Templeton DJ, Hannink M. Keap1 is a redox-regulated substrate adaptor protein for a

Cul3-dependent ubiquitin ligase complex. Mol Cell Biol 2004; 24:10941-53. [PMID: 15572695].

25. Datta S, Cano M, Ebrahimi K, Wang L, Handa JT. The impact of oxidative stress and inflammation on RPE degeneration in non-neovascular AMD. Prog Retin Eye Res 2017; •••:201-18. [PMID: 28336424].

26. Ambati J, Fowler BJ. Mechanisms of age-related macular degeneration. Neuron 2012; 75:26-39. [PMID: 22794258].

27. Cano M, Datta S, Wang L, Liu T, Flores-Bellver M, Sachdeva M, Sinha D, Handa JT. Nrf2 deficiency decreases NADPH from impaired IDH shuttle and pentose phosphate pathway in retinal pigmented epithelial cells to magnify oxidative stress-induced mitochondrial dysfunction. Aging Cell 2021; 20:e13444-[PMID: 34313391].

28. Wang L, Kondo N, Cano M, Ebrahimi K, Yoshida T, Barnett BP, Biswal S, Handa JT. Nrf2 signaling modulates cigarette smoke-induced complement activation in retinal pigmented epithelial cells. Free Radic Biol Med 2014; 70:155-66. [PMID: 24440594].

29. Sachdeva MM, Cano M, Handa JT. Nrf2 signaling is impaired in the aging RPE given an oxidative insult. Exp Eye Res 2014; 119:111-4. [PMID: 24216314].

30. Suzuki M, Betsuyaku T, Ito Y, Nagai K, Nasuhara Y, Kaga K, Kondo S, Nishimura M. Down-regulated NF-E2-related factor 2 in pulmonary macrophages of aged smokers and patients with chronic obstructive pulmonary disease. Am J Respir Cell Mol Biol 2008; 39:673-82. [PMID: 18566336].

31. Justilien V, Pang JJ, Renganathan K, Zhan X, Crabb JW, Kim SR, Sparrow JR, Hauswirth WW, Lewin AS. SOD2 knockdown mouse model of early AMD. Invest Ophthalmol Vis Sci 2007; 48:4407-20. [PMID: 17898259].

32. Seo SJ, Krebs MP, Mao H, Jones K, Conners M, Lewin AS. Pathological consequences of long-term mitochondrial oxidative stress in the mouse retinal pigment epithelium. Exp Eye Res 2012; 101:60-71. [PMID: 22687918].

33. Thampi P, Rao HV, Mitter SK, Cai J, Mao H, Li H, Seo S, Qi X, Lewin AS, Romano C, Boulton ME. The 5HT1a receptor agonist 8-Oh DPAT induces protection from lipofuscin accumulation and oxidative stress in the retinal pigment epithelium. PLoS One 2012; 7:e34468-[PMID: 22509307].

34. Brown EE, DeWeerd AJ, Ildefonso CJ, Lewin AS, Ash JD. Mitochondrial oxidative stress in the retinal pigment epithelium (RPE) led to metabolic dysfunction in both the RPE and retinal photoreceptors. Redox Biol 2019; 24:101201-[PMID: 31039480].

35. Mao H, Seo SJ, Biswal MR, Li H, Conners M, Nandyala A, Jones K, Le YZ, Lewin AS. Mitochondrial oxidative stress in the retinal pigment epithelium leads to localized retinal degeneration. Invest Ophthalmol Vis Sci 2014; 55:4613-27. [PMID: 24985474].

36. Chao JR, Knight K, Engel AL, Jankowski C, Wang Y, Manson MA, Gu H, Djukovic D, Raftery D, Hurley JB, Du J. Human retinal pigment epithelial cells prefer proline as a nutrient and transport metabolic intermediates to the retinal side. J Biol Chem 2017; 292:12895-905. [PMID: 28615447].

37. Hurley JB. Retina Metabolism and Metabolism in the Pigmented Epithelium: A Busy Intersection. Annu Rev Vis Sci 2021; 7:665-92. [PMID: 34102066].

38. Kanow MA, Giarmarco MM, Jankowski CS, Tsantilas K, Engel AL, Du J, Linton JD, Farnsworth CC, Sloat SR, Rountree A, Sweet IR, Lindsay KJ, Parker ED, Brockerhoff SE, Sadilek M, Chao JR, Hurley JB. Biochemical adaptations of the retina and retinal pigment epithelium support a metabolic ecosystem in the vertebrate eye. eLife 2017; 6:e28899-[PMID: 28901286].

39. Li B, Zhang T, Liu W, Wang Y, Xu R, Zeng S, Zhang R, Zhu S, Gillies MC, Zhu L, Du J. Metabolic Features of Mouse and Human Retinas: Rods versus Cones, Macula versus Periphery, Retina versus RPE. iScience. 2020;23:xxx.

40. Xu R, Ritz BK, Wang Y, Huang J, Zhao C, Gong K, Liu X, Du J. The retina and retinal pigment epithelium differ in nitrogen metabolism and are metabolically connected. J Biol Chem 2020; 295:2324-35. [PMID: 31953322].

41. Ahn B, Ranjit R, Premkumar P, Pharaoh G, Piekarz KM, Matsuzaki S, Claflin DR, Riddle K, Judge J, Bhaskaran S, Satara Natarajan K, Barboza E, Wronowski B, Kinter M, Humphries KM, Griffin TM, Freeman WM, Richardson A, Brooks SV, Van Remmen H. Mitochondrial oxidative stress impairs contractile function but paradoxically increases muscle mass via fibre branching. J Cachexia Sarcopenia Muscle 2019; 10:411-28. [PMID: 30706998].

42. Clerici S, Boletta A. Role of the KEAP1-NRF2 Axis in Renal Cell Carcinoma. Cancers (Basel) 2020; 12:3458-83. [PMID: 33233657].

43. Galicia-Moreno M, Lucano-Landeros S, Monroy-Ramirez HC, Silva-Gomez J, Gutierrez-Cuevas J, Santos A, Armendariz-Borunda J. Roles of Nrf2 in Liver Diseases: Molecular, Pharmacological, and Epigenetic Aspects. Antioxidants 2020; 9:[PMID: 33066023].

44. Martin-Montalvo A, Villalba JM, Navas P, de Cabo R. NRF2, cancer and calorie restriction. Oncogene 2011; 30:505-20. [PMID: 21057541].

45. Zhang D, Rennhack J, Andrechek ER, Rockwell CE, Liby KT. Identification of an Unfavorable Immune Signature in Advanced Lung Tumors from Nrf2-Deficient Mice. Antioxid Redox Signal 2018; 29:1535-52. [PMID: 29634345].

46. Zhao Z, Chen Y, Wang J, Sternberg P, Freeman ML, Grossniklaus HE, Cai J. Age-related retinopathy in NRF2-deficient mice. PLoS One 2011; 6:e19456-[PMID: 21559389].

47. Rowan S, Jiang S, Chang ML, Volkin J, Cassalman C, Smith KM, Streeter MD, Spiegel DA, Moreira-Neto C, Rabbani N, Thornalley PJ, Smith DE, Waheed NK, Taylor A. A low glycemic diet protects disease-prone Nrf2-deficient mice against age-related macular degeneration. Free Radic Biol Med 2020; 150:75-86. [PMID: 32068111].

48. Zhao Z, Xu P, Jie Z, Zuo Y, Yu B, Soong L, Sun J, Chen Y, Cai J. gammadelta T cells as a major source of IL-17 production

during age-dependent RPE degeneration. Invest Ophthalmol Vis Sci 2014; 55:6580-9. [PMID: 25212781].

49. Felszeghy S, Viiri J, Paterno JJ, Hyttinen JMT, Koskela A, Chen M, Leinonen H, Tanila H, Kivinen N, Koistinen A, Toropainen E, Amadio M, Smedowski A, Reinisalo M, Winiarczyk M, Mackiewicz J, Mutikainen M, Ruotsalainen AK, Kettunen M, Jokivarsi K, Sinha D, Kinnunen K, Petrovski G, Blasiak J, Bjorkoy G, Koskelainen A, Skottman H, Urtti A, Salminen A, Kannan R, Ferrington DA, Xu H, Levonen AL, Tavi P, Kauppinen A, Kaarniranta K. Loss of NRF-2 and PGC-1alpha genes leads to retinal pigment epithelium damage resembling dry age-related macular degeneration. Redox Biol 2019; 20:1-12. [PMID: 30253279].

50. Plafker SM, Plafker KS, Weissman AM, Macara IG. Ubiquitin charging of human class III ubiquitin-conjugating enzymes triggers their nuclear import. J Cell Biol 2004; 167:649-59. [PMID: 15545318].

51. Gong Y, Cao X, Gong L, Li W. Sulforaphane alleviates retinal ganglion cell death and inflammation by suppressing NLRP3 inflammasome activation in a rat model of retinal ischemia/reperfusion injury. Int J Immunopathol Pharmacol 2019; 33:2058738419861777-[PMID: 31266422].

52. Kong L, Liu B, Zhang C, Wang B, Wang H, Song X, Yang Y, Ren X, Yin L, Kong H, Ma H. The therapeutic potential of sulforaphane on light-induced photoreceptor degeneration through antiapoptosis and antioxidant protection. Neurochem Int 2016; 100:52-61. [PMID: 27567738].

53. Tanito M, Masutani H, Kim YC, Nishikawa M, Ohira A, Yodoi J. Sulforaphane induces thioredoxin through the antioxidant-responsive element and attenuates retinal light damage in mice. Invest Ophthalmol Vis Sci 2005; 46:979-87. [PMID: 15728556].

54. Wu DM, Ji X, Ivanchenko MV, Chung M, Piper M, Rana P, Wang SK, Xue Y, West E, Zhao SR, Xu H, Cicconet M, Xiong W, Cepko CL. Nrf2 overexpression rescues the RPE in mouse models of retinitis pigmentosa. JCI Insight 2021; 6:e145029-[PMID: 33491671].

55. Xiong W, MacColl Garfinkel AE, Li Y, Benowitz LI, Cepko CL. NRF2 promotes neuronal survival in neurodegeneration and acute nerve damage. J Clin Invest 2015; 125:1433-45. [PMID: 25798616].

56. Fleckenstein M, Keenan TDL, Guymer RH, Chakravarthy U, Schmitz-Valckenberg S, Klaver CC, Wong WT, Chew EY. Age-related macular degeneration. Nat Rev Dis Primers 2021; 7:31-[PMID: 33958600].

57. Toma C, De Cilla S, Palumbo A, Garhwal DP, Grossini E. Oxidative and Nitrosative Stress in Age-Related Macular Degeneration: A Review of Their Role in Different Stages of Disease. Antioxidants 2021; 10:653-73. [PMID: 33922463].

58. Punzo C, Kornacker K, Cepko CL. Stimulation of the insulin/mTOR pathway delays cone death in a mouse model of retinitis pigmentosa. Nat Neurosci 2009; 12:44-52. [PMID: 19060896].

59. Rogers BS, Symons RC, Komeima K, Shen J, Xiao W, Swaim ME, Gong YY, Kachi S, Campochiaro PA. Differential sensitivity of cones to iron-mediated oxidative damage. Invest Ophthalmol Vis Sci 2007; 48:438-45. [PMID: 17197565].

60. Ren X, Li C, Liu J, Zhang C, Fu Y, Wang N, Ma H, Lu H, Kong H, Kong L. Thioredoxin plays a key role in retinal neuropathy prior to endothelial damage in diabetic mice. Oncotarget 2017; 8:61350-64. [PMID: 28977868].

61. Komeima K, Rogers BS, Lu L, Campochiaro PA. Antioxidants reduce cone cell death in a model of retinitis pigmentosa. Proc Natl Acad Sci USA 2006; 103:11300-5. [PMID: 16849425].

62. Kang K, Yu M. Protective effect of sulforaphane against retinal degeneration in the Pde6(rd10) mouse model of retinitis pigmentosa. Curr Eye Res 2017; 42:1684-8. [PMID: 28937835].

63. Agbaga MP, Merriman DK, Brush RS, Lydic TA, Conley SM, Naash MI, Jackson S, Woods AS, Reid GE, Busik JV, Anderson RE. Differential composition of DHA and very-long-chain PUFAs in rod and cone photoreceptors. J Lipid Res 2018; 59:1586-96. [PMID: 29986998].

64. Frost LS, Mitchell CH, Boesze-Battaglia K. Autophagy in the eye: implications for ocular cell health. Exp Eye Res 2014; 124:56-66. [PMID: 24810222].

65. Zhou Z, Doggett TA, Sene A, Apte RS, Ferguson TA. Autophagy supports survival and phototransduction protein levels in rod photoreceptors. Cell Death Differ 2015; 22:488-98. [PMID: 25571975].

66. Zhou Z, Vinberg F, Schottler F, Doggett TA, Kefalov VJ, Ferguson TA. Autophagy supports color vision. Autophagy 2015; 11:1821-32. [PMID: 26292183].

67. Yang PM, Cheng KC, Huang JY, Wang SY, Lin YN, Tseng YT, Hsieh CW, Wung BS. Sulforaphane inhibits blue light-induced inflammation and apoptosis by upregulating the SIRT1/PGC-1alpha/Nrf2 pathway and autophagy in retinal pigment epithelial cells. Toxicol Appl Pharmacol 2021; 421:115545-[PMID: 33894213].

68. Lu Y, Zhang Y, Lou Y, Cui W, Miao L. Sulforaphane suppresses obesity-related glomerulopathy-induced damage by enhancing autophagy via Nrf2. Life Sci 2020; 258:118153-[PMID: 32738361].

69. Zheng K, Ma J, Wang Y, He Z, Deng K. Sulforaphane Inhibits Autophagy and Induces Exosome-Mediated Paracrine Senescence via Regulating mTOR/TFE3. Mol Nutr Food Res 2020; 64:e1901231-[PMID: 32476238].

70. Qiu Y, Yao J, Jia L, Thompson DA, Zacks DN. Shifting the balance of autophagy and proteasome activation reduces proteotoxic cell death: a novel therapeutic approach for restoring photoreceptor homeostasis. Cell Death Dis 2019; 10:547-[PMID: 31320609].

71. Briones-Herrera A, Ramirez-Camacho I, Zazueta C, Tapia E, Pedraza-Chaverri J. Altered proximal tubule fatty acid utilization, mitophagy, fission and supercomplexes arrangement in experimental Fanconi syndrome are ameliorated by

sulforaphane-induced mitochondrial biogenesis. Free Radic Biol Med 2020; 153:54-70. [PMID: 32315768].

72. Lei P, Tian S, Teng C, Huang L, Liu X, Wang J, Zhang Y, Li B, Shan Y. Sulforaphane Improves Lipid Metabolism by Enhancing Mitochondrial Function and Biogenesis In Vivo and In Vitro. Mol Nutr Food Res 2021; 65:e2170023-[PMID: 34085388].

73. Li D, Shao R, Wang N, Zhou N, Du K, Shi J, Wang Y, Zhao Z, Ye X, Zhang X, Xu H. Sulforaphane Activates a lysosome-dependent transcriptional program to mitigate oxidative stress. Autophagy 2021; 17:872-87. [PMID: 32138578].

74. Ambrecht LA, Perlman JI, McDonnell JF, Zhai Y, Qiao L, Bu P. Protection of retinal function by sulforaphane following retinal ischemic injury. Exp Eye Res 2015; 138:66-9. [PMID: 26142954].

75. Pan H, He M, Liu R, Brecha NC, Yu AC, Pu M. Sulforaphane protects rodent retinas against ischemia-reperfusion injury through the activation of the Nrf2/HO-1 antioxidant pathway. PLoS One 2014; 9:e114186-[PMID: 25470382].

76. Kong L, Tanito M, Huang Z, Li F, Zhou X, Zaharia A, Yodoi J, McGinnis JF, Cao W. Delay of photoreceptor degeneration in tubby mouse by sulforaphane. J Neurochem 2007; 101:1041-52. [PMID: 17394579].

77. Li S, Yang H, Chen X. Protective effects of sulforaphane on diabetic retinopathy: activation of the Nrf2 pathway and inhibition of NLRP3 inflammasome formation. Exp Anim 2019; 68:221-31. [PMID: 30606939].

78. Lv J, Bao S, Liu T, Wei L, Wang D, Ye W, Wang N, Song S, Li J, Chudhary M, Ren X, Kong L. Sulforaphane delays diabetes-induced retinal photoreceptor cell degeneration. Cell Tissue Res 2020; 382:477-86. [PMID: 32783101].

79. Cai X, Nash Z, Conley SM, Fliesler SJ, Cooper MJ, Naash MI. A partial structural and functional rescue of a retinitis pigmentosa model with compacted DNA nanoparticles. PLoS One 2009; 4:e5290-[PMID: 19390689].

80. Wert KJ, Velez G, Kanchustambham VL, Shankar V, Evans LP, Sengillo JD, Zare RN, Bassuk AG, Tsang SH, Mahajan VB. Metabolite therapy guided by liquid biopsy proteomics delays retinal neurodegeneration. EBioMedicine 2020; 52:102636-[PMID: 32028070].

81. Sui YB, Zhang KK, Ren YK, Liu L, Liu Y. The role of Nrf2 in astragaloside IV-mediated antioxidative protection on heart failure. Pharm Biol 2020; 58:1192-8. [PMID: 33253607].

82. Fukunaga N, Kawajiri H, Badiwala MV, Butany J, Li RK, Billia F, Rao V. Protective role of Nrf2 against ischemia reperfusion injury and cardiac allograft vasculopathy. Am J Transplant 2020; 20:1262-71. [PMID: 31769924].

83. Miao L, St Clair DK. Regulation of superoxide dismutase genes: implications in disease. Free Radic Biol Med 2009; 47:344-56. [PMID: 19477268].

84. Holmstrom KM, Kostov RV, Dinkova-Kostova AT. The multi-faceted role of Nrf2 in mitochondrial function. Curr Opin Toxicol. 2016; 1:80-91. [PMID: 28066829].

85. Hurley JB, Lindsay KJ, Du J. Glucose, lactate, and shuttling of metabolites in vertebrate retinas. J Neurosci Res 2015; 93:1079-92. [PMID: 25801286].

86. Kurihara T, Westenskow PD, Gantner ML, Usui Y, Schultz A, Bravo S, Aguilar E, Wittgrove C, Friedlander M, Paris LP, Chew E, Siuzdak G, Friedlander M. Hypoxia-induced metabolic stress in retinal pigment epithelial cells is sufficient to induce photoreceptor degeneration. eLife 2016; 5:e14319-[PMID: 26978795].

87. Swarup A, Samuels IS, Bell BA, Han JYS, Du J, Massenzio E, Abel ED, Boesze-Battaglia K, Peachey NS, Philp NJ. Modulating GLUT1 expression in retinal pigment epithelium decreases glucose levels in the retina: impact on photoreceptors and Muller glial cells. Am J Physiol Cell Physiol 2019; 316:C121-33. [PMID: 30462537].

88. Ingram NT, Fain GL, Sampath AP. Elevated energy requirement of cone photoreceptors. Proc Natl Acad Sci USA 2020; 117:19599-603. [PMID: 32719136].

89. Macaluso C, Onoe S, Niemeyer G. Changes in glucose level affect rod function more than cone function in the isolated, perfused cat eye. Invest Ophthalmol Vis Sci 1992; 33:2798-808. [PMID: 1526729].

90. Nihira M, Anderson K, Gorin FA, Burns MS. Primate rod and cone photoreceptors may differ in glucose accessibility. Invest Ophthalmol Vis Sci 1995; 36:1259-70. [PMID: 7775103].

91. Baik AH, Jain IH. Turning the Oxygen Dial: Balancing the Highs and Lows. Trends Cell Biol 2020; 30:516-36. [PMID: 32386878].

92. Jain IH, Zazzeron L, Goldberger O, Marutani E, Wojtkiewicz GR, Ast T, Wang H, Schleifer G, Stepanova A, Brepoels K, Schoonjans L, Carmeliet P, Galkin A, Ichinose F, Zapol WM, Mootha VK. Leigh Syndrome Mouse Model Can Be Rescued by Interventions that Normalize Brain Hyperoxia, but Not HIF Activation. Cell Metab 2019; 30:824-32. .

93. Jain IH, Zazzeron L, Goli R, Alexa K, Schatzman-Bone S, Dhillon H, Goldberger O, Peng J, Shalem O, Sanjana NE, Zhang F, Goessling W, Zapol WM, Mootha VK. Hypoxia as a therapy for mitochondrial disease. Science 2016; 352:54-61. [PMID: 26917594].

94. Liu GY, Sabatini DM. mTOR at the nexus of nutrition, growth, ageing and disease. Nat Rev Mol Cell Biol 2020; 21:183-203. [PMID: 31937935].

95. Rosales MAB, Shu DY, Iacovelli J, Saint-Geniez M. Loss of PGC-1alpha in RPE induces mesenchymal transition and promotes retinal degeneration. Life Sci Alliance. 2019;2.

96. Zhao C, Yasumura D, Li X, Matthes M, Lloyd M, Nielsen G, Ahern K, Snyder M, Bok D, Dunaief JL, LaVail MM, Vollrath D. mTOR-mediated dedifferentiation of the retinal pigment epithelium initiates photoreceptor degeneration in mice. J Clin Invest 2011; 121:369-83. [PMID: 21135502].

97. Go YM, Zhang J, Fernandes J, Litwin C, Chen R, Wensel TG, Jones DP, Cai J, Chen Y. MTOR-initiated metabolic switch

and degeneration in the retinal pigment epithelium. FASEB J 2020; 34:12502-20. [PMID: 32721041].

98. Huang J, Gu S, Chen M, Zhang SJ, Jiang Z, Chen X, Jiang C, Liu G, Radu RA, Sun X, Vollrath D, Du J, Yan B, Zhao C. Abnormal mTORC1 signaling leads to retinal pigment epithelium degeneration. Theranostics 2019; 9:1170-80. [PMID: 30867823].

99. Lei P, Tian S, Teng C, Huang L, Liu X, Wang J, Zhang Y, Li B, Shan Y. Sulforaphane Improves Lipid Metabolism by Enhancing Mitochondrial Function and Biogenesis In Vivo and In Vitro. Mol Nutr Food Res 2019; 63:e1800795-[PMID: 30578708].

100. Negrette-Guzman M, Huerta-Yepez S, Vega MI, Leon-Contreras JC, Hernandez-Pando R, Medina-Campos ON, Rodriguez E, Tapia E, Pedraza-Chaverri J. Sulforaphane induces differential modulation of mitochondrial biogenesis and dynamics in normal cells and tumor cells. Food Chem Toxicol 2017; 100:90-102. [PMID: 27993529].

101. Pan WW, Wubben TJ, Besirli CG. Photoreceptor metabolic reprogramming: current understanding and therapeutic implications. Commun Biol. 2021; 4:245-[PMID: 33627778].

102. Rajala A, Wang Y, Rajala RVS. Constitutive Activation Mutant mTOR Promote Cone Survival in Retinitis Pigmentosa Mice. Adv Exp Med Biol 2018; 1074:491-7. [PMID: 29721981].

103. Venkatesh A, Ma S, Le YZ, Hall MN, Ruegg MA, Punzo C. Activated mTORC1 promotes long-term cone survival in retinitis pigmentosa mice. J Clin Invest 2015; 125:1446-58. [PMID: 25798619].

104. Holmstrom KM, Baird L, Zhang Y, Hargreaves I, Chalasani A, Land JM, Stanyer L, Yamamoto M, Dinkova-Kostova AT, Abramov AY. Nrf2 impacts cellular bioenergetics by controlling substrate availability for mitochondrial respiration. Biol Open 2013; 2:761-70. [PMID: 23951401].

Articles are provided courtesy of Emory University and the Zhongshan Ophthalmic Center, Sun Yat-sen University, P.R. China. The print version of this article was created on 16 October 2022. This reflects all typographical corrections and errata to the article through that date. Details of any changes may be found in the online version of the article.